Inorganic Chemistry

Article

pubs.acs.org/IC

Cooperative Electronic and Structural Regulation in a Bioinspired Allosteric Photoredox Catalyst

Alejo M. Lifschitz,[†,§] Ryan M. Young,[†,‡] Jose Mendez-Arroyo,[†] C. Michael McGuirk,[†] Michael R. Wasielewski,*[,†,‡] and Chad A. Mirkin*[,†,‡]

[†]Department of Chemistry and International Institute for Nanotechnology and [‡]Argonne-Northwestern Solar Energy Research (ANSER) Center, Northwestern University, 2145 Sheridan Road, Evanston, Illinois 60208, United States

Supporting Information

ABSTRACT: Herein, we report the first allosteric photoredox catalyst regulated via constructively coupled structural and electronic control. While often synergistically exploited in nature, these two types of control mechanisms have only been applied independently in the vast majority of allosteric enzyme mimics and receptors in the literature. By embedding a model of photosystem II in a supramolecular coordination complex that responds to chloride as an allosteric effector, we show that distance and electronic control of light harvesting can be married to maximize allosteric regulation of catalytic activity. This biomimetic system is composed of a Bodipy photoantenna, which is capable of transferring excited-state energy to a photoredox pair, wherein the excitation energy is used to generate a catalytically active charge-separated state. The structural aspect of allosteric regulation is achieved by toggling the coordination chemistry of an antenna-functionalized hemilabile ligand via partial displacement from a Rh^{I} structual node using chloride. In doing so, the distance between the antenna and the central photoredox catalyst is increased, lowering the inherent efficiency of through-space energy transfer. At the same time, coordination of chloride lowers both the charge of the Rh^{I} node and the reduction potential of the $Rh^{II/I}$ couple, to the extent that electronic quenching of the antenna excited state is possible via photoinduced electron transfer from the metal center. Compared to a previously developed system that operates solely via electronic regulation, the present system demonstrates that coupling electronic and structural approaches to allosteric regulation gives rise to improved switching ratios between catalytically active and inactive states. Contributions from both structural and electronic control mechanisms are probed via nuclear magnetic resonance, X-ray diffraction, electrochemical, spectroelectrochemical, and transient absorption studies. Overall, this work establishes that intertwined electronic and structural regulatory mechanisms can be borrowed from nature to build stimuli-responsive inorganic materials with potential applications in sensing, catalysis, and photonic devices.

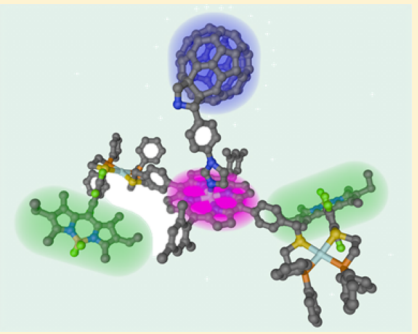

INTRODUCTION

Allosteric enzyme mimics exploit simple chemical inputs to reversibly effect large changes in the physical, chemical, and electronic properties of inorganic materials.[1,2] Abiotic allosteric constructs have thus been applied to the development of molecular sensors[3] and signal amplification devices,[4] as well as to the control of challenging chemical reactions.[5] To do so, the majority of allosteric receptors and catalysts in the literature have made use of structural-based regulation, wherein activity is controlled via changes in the shape or steric confinement around active moieties.[6] On the other hand, regulation of catalysts, allosteric or otherwise, based on electron-transfer and light-harvesting processes has generally been possible by using control mechanisms that instead tailor the electronic state of the active site.[7−9] In natural systems, however, structural and electronic regulatory strategies often act synergistically to maximize the toggling between active states, with photosystem II (PSII) being a prime example (Figure 1A).[10−13] Photoactive systems are indeed good targets for coupled regulatory strategies because the interactions between their active components are not only dependent on the electronic environment[14,15] but also highly sensitive to structural cues given the fundamental distance dependence of through-space phenomena such as electron and energy transfer.[16,17] The challenge has thus been to develop regulatory strategies to control inorganic catalysts by constructively harnessing the electronic and structural perturbations that occur upon analyte binding to an allosteric framework.

Herein, we describe one such strategy, in which a photoredox catalyst composed of light-harvesting antenna (LHA) and reaction center (RC) mimics of PSII is allosterically regulated between catalytically active and inactive states by controlling both the distance between the active units and the electronic state of the antenna, reminiscent of the coupled structural and electronic regulation of the light-harvesting complex II (LHCII) of PSII by the thylakoid PsbS protein (Figure 1A).[10] This stimuli-responsive construct [$(\mathbf{1-2})\bullet\mathbf{ImC_{60}}$; Figure 1B] shows for the first time that bioinspired regulatory strategies based on constructive electronic and structural

Received: January 13, 2016

DOI: 10.1021/acs.inorgchem.6b00095
Inorg. Chem. XXXX, XXX, XXX−XXX

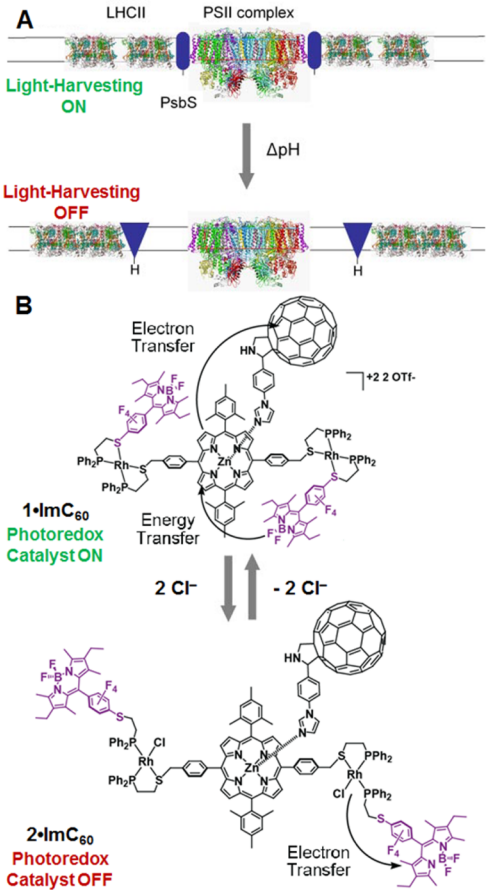

Figure 1. Regulation of light harvesting via coupled structural and electronic changes in antenna complexes induced by recognition events in PSII (A, adapted from ref 10) and in allosteric, inorganic photoredox catalyst **(1−2)•ImC$_{60}$** (B).

control can be applied to the reversible and in situ regulation of inorganic photoredox catalysts.

LHA−RC mimics have often been built using a Bodipy LHA, which can transfer excitation energy to a porphyrin-C$_{60}$ RC, wherein the excitation energy drives the formation of a catalytically active charge-separated state.[18] We recently reported a LHA−RC mimic of this kind, **(3−4)•ImC$_{60}$** (Scheme 1), whose activity is allosterically controlled through the coordination chemistry of hemilabile LHA ligands.[7] In particular, chelation of a Bodipy hemilabile ligand to a charged Rh^{I} node in **4•ImC$_{60}$** increases the LHA redox potential relative to that of the Rh$^{II/I}$ couple, thereby quenching the light-harvesting activity in the closed coordination state via photoinduced electron transfer (PET).[19] Toggling with mild, nonredox active inputs uniquely enables in situ and reversible regulation of photoredox catalytic activity. A critical drawback of this switch, however, depends on the fact that light harvesting is promoted as the distance between the LHA and RC increases, which lowers the intrinsic efficiency of energy transfer in the active state and, consequently, curtails the catalytic switching ratio. We thus hypothesized that a reverse system, in which quenching occurs in the open state, would constructively couple structural and electronic changes and maximize allosteric switching capabilities. This is readily achieved herein by applying discrete synthetic modifications on the hemilabile antenna ligand that fundamentally change the

Scheme 1. Previously Developed LHA−RC Mimic (3−4)•ImC$_{60}$, Which Regulates Activity Solely via Electronic Control of the LHA (Adapted from Reference 7)

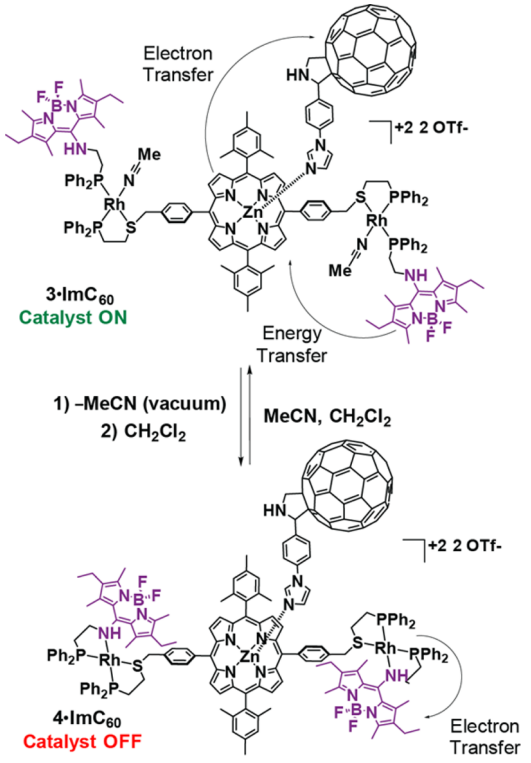

structure−function relationship of the biomimetic allosteric catalyst.

RESULTS AND DISCUSSION

Assembly and Structural Regulation. **(1−2)•ImC$_{60}$** was assembled in a modular fashion by first incorporating porphyrin- and Bodipy-functionalized hemilabile ligands **5**[7] and **6**[20] into **2** (Scheme 2). This Rh^{I} complex was quantitatively assembled via the weak-link approach (WLA), a synthetic strategy that makes use of hemilabile ligands and structural d^{8} metal centers to produce structurally switchable, multifunctional coordination frameworks.[1,4] The key to accessing such structures selectively and quantitatively is the use of halide-containing d^{8} transition-metal precursors and sets of hemilabile ligands with markedly different chelating strengths. In the system discussed herein, the relatively lower chelating strength of the LHA ligand, resulting from the perfluorinated phenyl meso substituent, is key to yielding **2** exclusively rather than a mixture of all possible ligand−Rh^{I} combinations. Selective formation of **2** is also contingent upon the stabilization of homoligated complexes of each ligand in solution, which form prior to halide-induced rearrangement into the target heteroligated construct.[21] This is achieved by appending solubilizing mesityl and alkyl groups around the photoactive units in **5** and **6** that prevent precipitation of dimer structures. Chloride abstraction from **2** via precipitation with Tl^{I} quantitatively affords closed complex **1**, thereby increasing the charge of the Rh^{I} coordination spheres to 1+ while concomitantly lowering the distance between the embedded components by ∼15 Å (Figure 2). The cycle of chloride abstraction with Tl^{I} and reintroduction via the addition of

DOI: 10.1021/acs.inorgchem.6b00095
Inorg. Chem. XXXX, XXX, XXX−XXX

Scheme 2. Synthesis of Light-Harvesting Switch 1−2

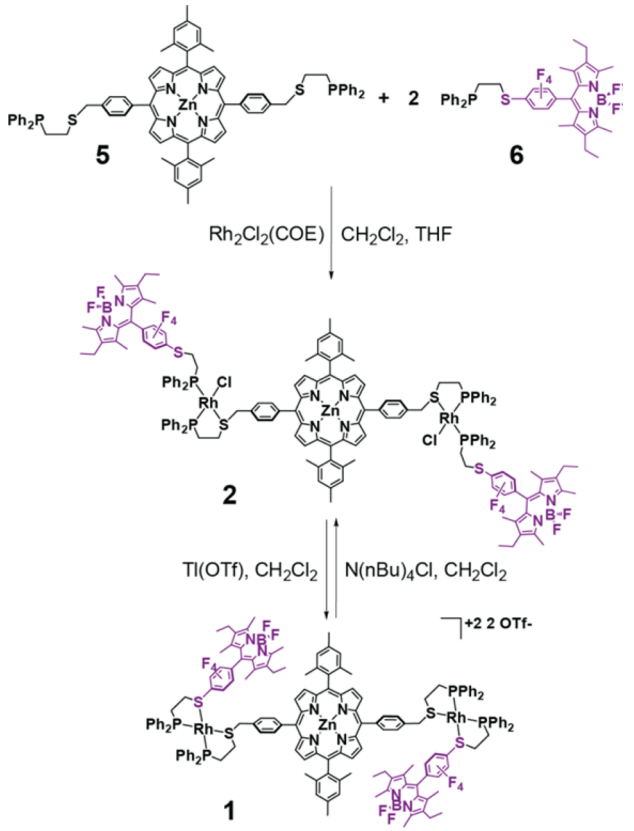

$N(nBu)_4Cl$ can be repeated to reversibly toggle between the two coordination states.

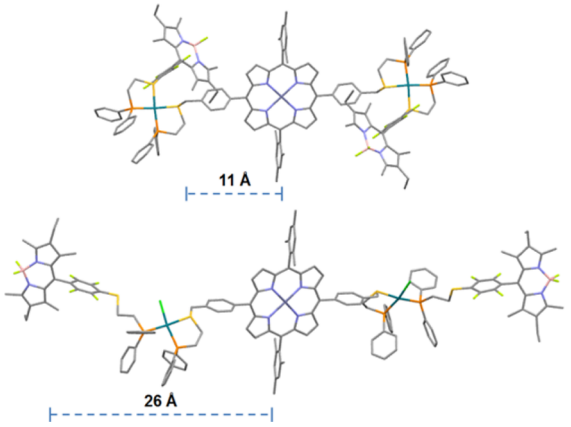

Figure 2. Solid-state structure of **1** (top, adapted from ref 7) and theoretical model of **2** obtained from geometry optimization using PBE0 with TZ2P basis sets. H atoms and counteranions are omitted. Color code: Rh, green; Cl, light green; S, yellow; P, orange; N, blue; B, pink; F, light yellow; C, gray; Zn, dark blue.

The benzyl bridge makes **5** a stronger chelator than **6** while also introducing a structural kink that exposes the Zn^{II} centers regardless of differences in steric confinement between **1** and **2**. Thus, a fullerene moiety with a long imidazole arm (**ImC_{60}**)[22] can be incorporated to similar degrees by both **1** ($K_{a,Im-Zn} = 4.1 \times 10^5\ M^{-1}$) and **2** ($K_{a,Im-Zn} = 1.9 \times 10^5\ M^{-1}$), as determined via UV−visible spectroscopy titration studies (see Figures S1 and S2). The toggling between coordination states using chloride as an allosteric effector, studied in **1** and **2** via fluorescence spectroscopy (Figures S3 and S4), is also possible in the presence of **ImC_{60}**. That is, even though saturation of all Zn^{II} sites requires an excess of the imidazole ligand, the excess does not interfere with coordination of the Rh^{I} center, as determined via ^{31}P NMR spectroscopy of **(1−2)•ImC_{60}** (see Figure S5). Furthermore, the coordination state of the Rh^{I} nodes can be addressed in the full LHA−RC assembly by abstracting chloride with Tl^{I} and subsequently reintroducing chloride as $N(nBu)_4Cl$, and the coordination transformations do not significantly affect the association between Zn^{II} and the fullerene−imidazole ligand (see Figure S5). These observations demonstrate that the orthogonality between the coordination chemistry of Rh^{I} and Zn^{II} can be exploited to selectively assemble and structurally toggle **(1−2)•ImC_{60}**.

Electronic Regulation. Modification of the antenna ligand previously used in **(3−4)•ImC_{60}** with a meso perfluorinated phenylene bridge, as in **(1−2)•ImC_{60}**, was hypothesized to preclude major inductive contributions from the hemilabile moiety on Bodipy upon formation of the Rh^{I}−S bond.[23] In doing so, we expected the redox properties of the antenna to remain constant upon changes in coordination to the Rh^{I} center. Thus, electronic regulation of light harvesting would be achieved by controlling the redox properties of Rh^{I}, specifically enabling quenching of the antenna excited state via PET by lowering the potential of the $Rh^{II/I}$ redox couple. By comparison, **(3−4)•ImC_{60}** achieves electronic regulation via PET by shifting the redox potential of the antenna rather than by changing the redox properties of the metal center. Consistent with our hypothesis, the cyclic voltammogram of **2** shows that, as a result of coordination of chloride, Rh^{I} is irreversibly oxidized at a potential that is 320 mV lower than the potential required to oxidize Bodipy (Figure 3A).[24] As a result, excitation of the Bodipy antenna yields minimal energy-transfer-based fluorescence from the zinc porphyrin moiety at 650 nm (Figure 3B), indicating that PET from Rh^{I} to Bodipy is able to outcompete energy transfer. On the other hand, chloride abstraction to give **1** increases the potential of the $Rh^{II/I}$ redox couple beyond the redox window of the LHA (Figure 3A), which is itself largely unaffected by the coordination change. As a result, the thermodynamic driving force for PET is removed and excitation of the antenna in **1** yields markedly enhanced fluorescence from the porphyrin moiety. Single-point calculations show that the changing electronic landscape of **1** and **2** arises from the effect that the coordination mode has on the Rh^{I} d_{z^2} orbital energy (see Figures S6 and S7). Specifically, chloride coordination raises the energy of the d_{z^2} orbital to the degree that it lies higher in energy than the Bodipy-center highest occupied molecular orbital (HOMO), suggesting that PET from the Rh^{I} center to the Bodipy excited state is thermodynamically possible in **2**. Transient absorption (TA) spectroscopy studies of **2** reveal that the rate of energy transfer is $1.0 \times 10^9\ s^{-1}$, while quenching via PET in a model LHA−Rh^{I} complex (**M2**; Scheme 3) occurs with a rate of $1.4 \times 10^{10}\ s^{-1}$ (see the Experimental Section for details). This observation suggests that regulation of energy transfer by triggering PET is possible because the quenching mechanism is kinetically faster by about an order of magnitude.

Overall, the toggling of PET and distances in **1** and **2** results in a 19-fold energy-transfer-efficiency switching ratio. This value is approximated from the changes in the lifetime of the excited antenna in **1** and **2** (see Table S1) relative to LHA−Rh^{I} complexes **M1** and **M2**,[19] in which the zinc porphyrin unit is

DOI: 10.1021/acs.inorgchem.6b00095
Inorg. Chem. XXXX, XXX, XXX−XXX

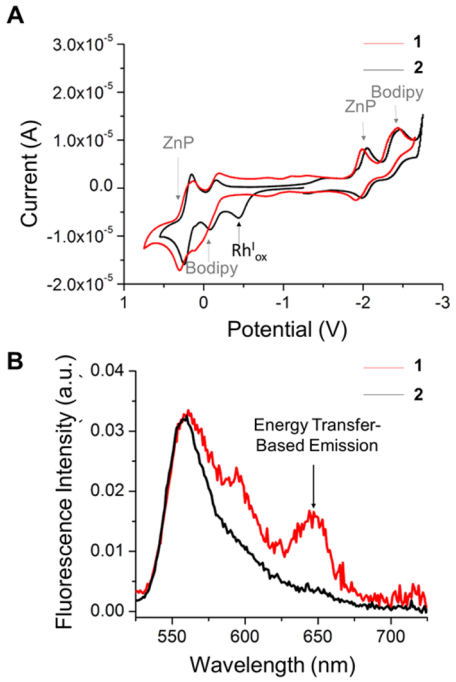

Figure 3. Use of chloride as an allosteric effector enabling regulation of the redox potential of the Rh^I center, thereby controlling the antenna's light-harvesting and energy-transfer capabilities. (A) Cyclic voltammograms of complexes **1** and **2** (potential vs Fc/Fc^+, CH_2Cl_2). (B) Emission spectra of complexes **1** and **2**, resulting from selective excitation of the Bodipy antenna (λ_{ex} = 505 nm, CH_2Cl_2).

Scheme 3. Previously Developed Model Complexes M1 and M2

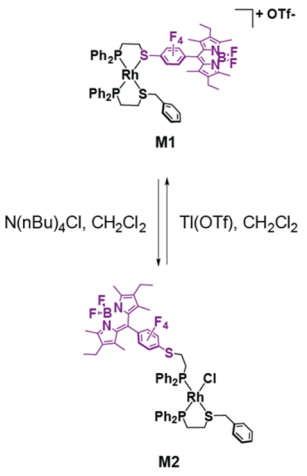

replaced by a benzyl group (Scheme 3; see the Experimental Section for details on calculation of the energy-transfer efficiencies). The contribution of structural regulation to this switching ratio corresponds to a 25% increase in the theoretical energy-transfer efficiency. That is, the theoretical energy-transfer efficiency changes from 71% for **1** to 57% for **2**. The theoretical values were calculated based on (1) changes in the distance between the antenna and porphyrin derived from the solid-state structure of **1** and a theoretical model of **2** (Figure 2) and (2) on the spectral overlap between the absorbance spectrum of **5** and the fluorescence spectrum of either **M1** or **M2** (see the Experimental Section for calculation details). This means that, under this distance regime, the main contributor to the switching ratio is electronic regulation via PET rather than structural control. Nevertheless, coupling of conformational and electronic changes allows **1** and **2** to outperform the energy-transfer switching capabilities of **3** and **4**, in which a 4-fold efficiency ratio is achieved (or 11-fold when accounting for changes in the antenna molar absorptivity).[7] Interestingly, the benzyl spacer in ligand **5** ensures that through-bond electronic communication between the porphyrin and the rest of the complex is minimized;[25] therefore, the excited-state lifetime of the energy acceptor is relatively constant following excitation of the antenna [$\tau_{ZnPorphyrin^*} = (1.15 \pm 0.08) \times 10^{-9}$ s in **1** and $(9.85 \pm 1.38) \times 10^{-10}$ s in **2**]. The energy states of complexes **1** and **2** that dictate the ability to regulate energy transfer via PET are displayed in Figure 4 and Table 1.

Allosteric Regulation of the Catalytic Activity. The near-IR (NIR)−TA spectra of **(1−2)•ImC$_{60}$** show that, upon excitation of Bodipy at λ_{ex} = 505 nm, generation of charge-separated species comprising the porphyrin and C_{60} moieties is most pronounced in the closed coordination state (Figure S13). Indeed, the TA spectra of **1•ImC$_{60}$** display a larger feature at 1010 nm characteristic of $C_{60}^{\bullet-}$.[22] To determine whether antenna design also reversed the catalytic activity of the photoredox complexes, we compared their ability to catalyze an electron-transfer reaction between methyl viologen hexafluorophosphate (MV) and 1-benzyl-1,4-dihydronicotinamide (BNAH).[26] It was found that complex **1•ImC$_{60}$** can drive the model photoredox reaction with an initial zero-order catalytic rate of $k = (1.2 \pm 0.1) \times 10^{-8}$ M s^{-1} when a 1 μM catalyst concentration and an excitation source with λ_{ex} = 505 nm and an excitation power of 0.8 mW are employed (see Figure S14). The rate was determined by tracking changes in absorbance at λ = 630 nm, indicative of the formation of reduced MV species. While absorbance at λ = 630 nm initially displayed a linear increase through time following excitation, Figure S14 shows that this relationship is not linear at longer excitation times. This is likely the result of a competing back-electron-transfer reaction that takes place as more reduced MV accumulates. Thus, the zero-order rate reported above represents an initial measure of the forward photoredox reaction rate prior to competition by reoxidation of MV. On the other hand, deviation from the linear regime could be a result of the short lifetime of the catalytically active charge-separated state, which limits the catalytic rate based on the diffusion kinetics at lower reactant concentrations. When the same experiment was carried out employing **2•ImC$_{60}$** as a catalyst, the initial zero-order catalytic rate was calculated to be $k = (1.6 \pm 0.2) \times 10^{-9}$ M s^{-1}, demonstrating that enabling PET from Rh^I to the excited state of the antenna in **2•ImC$_{60}$** results in a significant decrease in the ability to catalyze the model photoredox reaction. It should be noted that the photoredox reaction rates are dependent on the catalyst concentration and excitation power, and thus the calculated values are herein being used only for the sake of comparison between the two coordination states of the photoredox catalyst.

Finally, we compared the ability of the photoredox frameworks **(1−2)•ImC$_{60}$** and **(3−4)•ImC$_{60}$** to allosterically regulate the model electron-transfer reaction between MV and BNAH. As detailed in Figure 5, allosteric regulation experiments were carried out with 5 μM concentrations of either closed complex **1** or **4** and 10 equiv of **ImC$_{60}$**. After undergoing a period of irradiation at a wavelength where each antenna can be selectively excited (λ_{ex} = 505 nm for **1** and λ_{ex} = 480 nm for **4**), an allosteric effector was introduced to open the

DOI: 10.1021/acs.inorgchem.6b00095
Inorg. Chem. XXXX, XXX, XXX−XXX

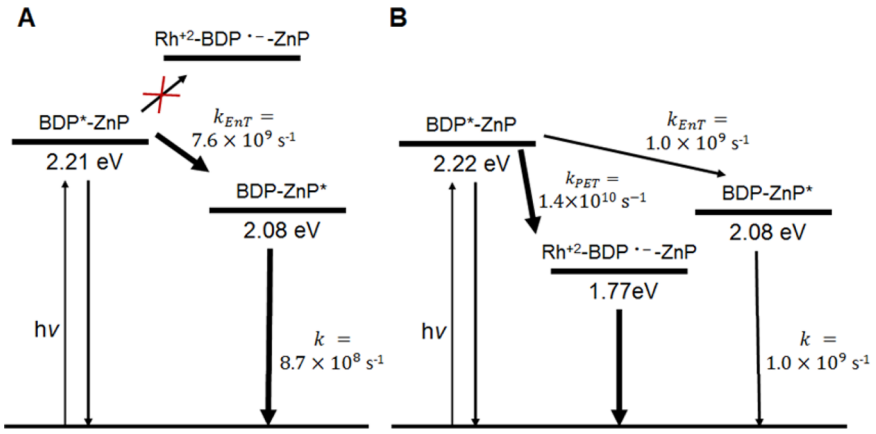

Figure 4. Energy-state diagrams of complexes **1** (A) and **2** (B) showing the relevant energies for energy transfer from the Bodipy excited state to the porphyrin and PET from Rh^{I} to the Bodipy excited state. The energies of the Bodipy and porphyrin excited states were determined from the emission spectra of **1** and **2**. The energies of the charge-separated states following PET were calculated as reported in a related system[22] using the irreversible anodic oxidation potential as an estimation for the reduction potential of the $Rh^{II/I}$ redox couple. k_{PET} was calculated from model complex **M2**.

Table 1. Electrochemical and Thermodynamic Data

complex	$E_{0,0,Bodipy}$ (eV)	$E^{\circ}_{Bodipy^{\bullet+}/Bodipy}$ (V)	$E_{1/2,Rh^{II/I}}$[a] (V)	$E^{\circ}_{Bodipy/Bodipy^{\bullet-}}$ (V)	ΔG_{EnT}[b] (eV)	$\Delta G_{PET\ Rh^{I}\text{-}Bodipy^{\bullet}}$[c] (eV)
1	0.067	−0.099		−2.349	−0.130	>0
2	0.048	−0.118	−0.438	−2.389	−0.138	−0.445

[a]The reduction potential for the $Rh^{II/I}$ redox couple was estimated from the irreversible anodic oxidation potential. [b]ΔG_{EnT} was calculated from the difference in energy between the Bodipy singlet excited state and the zinc porphyrin singlet excited state. [c]ΔG_{PET} was calculated from the Weller equation, as reported for a related system.[22]

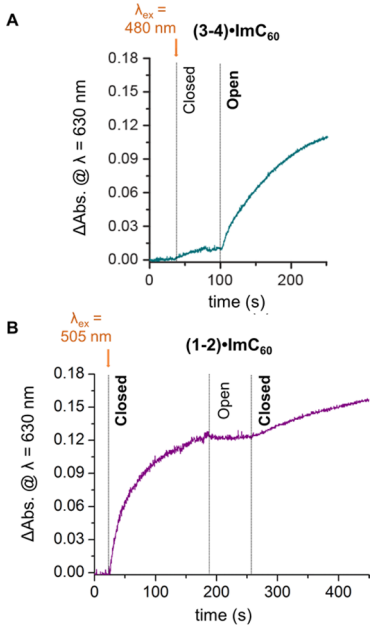

Figure 5. Allosteric regulation of a model electron-transfer reaction between MV and BNAH tracked by changes in the absorbance at 630 nm in the presence of a 5 μM CH_2Cl_2 solution of **3** and **4** (A; λ_{ex} = 480 nm, 0.8 mW, adapted from ref 7) or **1** and **2** (B; λ_{ex} = 505 nm, 0.8 mW) with 10 equiv of ImC_{60}. The initial concentration of both MV and BNAH employed was 0.1 mM.

coordination framework and changes in the rate of MV reduction were observed. Specifically, the previously reported switch **(3−4)•ImC$_{60}$** only displays a modest enhancement in the catalytic rate upon in situ framework expansion from closed **4•ImC$_{60}$** to open complex **3•ImC$_{60}$** via the introduction of 50 μL of MeCN as an allosteric input (Figure 5A).[7] On the other hand, the system presented herein displays enhanced photoredox activity in the closed coordination state **1•ImC$_{60}$**, which is markedly reduced upon the introduction of 2 equiv of chloride and the formation of **2•ImC$_{60}$** (Figure 5B). On a qualitative basis, Figure 5 shows that the allosteric switching ratio is more pronounced in the presently discussed **(1−2)•ImC$_{60}$** coordination framework, which parallels the quantified improvement in the energy-transfer switching ratio that results from coupled electronic and structural control.

CONCLUSIONS

We have demonstrated that the activity of a LHA−RC photoredox catalyst can be controlled with reversible chemical inputs by modulating the LHA−RC distance and PET from the allosteric center. As described throughout this article and summarized in Figure 6, the synthesis and switchability of **(1−2)•ImC$_{60}$** is based on several structural and electronic design considerations that are highly intertwined. For instance, the selective and quantitative formation of complex **2** is possible given that the antenna and energy acceptor are functionalized with solubilizing groups and hemilabile ligands of different coordinating strength. At the same time, these modifications optimize the redox potential of the antenna so that it can be quenched via PET only in the expanded coordination state, in addition to tuning the antenna HOMO−LUMO gap to achieve energy transfer to the central porphyrin unit. In the case of the porphyrin ligand, the relatively less electron-withdrawing benzyl bridge introduces a structural kink, which allows for coordination to the central porphyrin unit by exploiting the orthogonal coordination behavior of Zn^{II} compared to the Rh^{I} structural and electronic regulator. This series of considerations clearly shows that, just as in natural systems, structural and

DOI: 10.1021/acs.inorgchem.6b00095
Inorg. Chem. XXXX, XXX, XXX−XXX

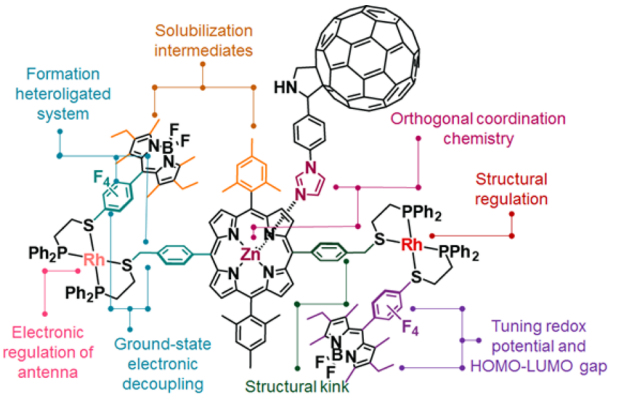

Figure 6. Intertwined structural and electronic design considerations enabling the synthesis and allosteric switching of **1**−**2**•**ImC$_{60}$**.

electronic effects must be leveraged against each other to optimize the catalytic and regulatory properties.

Regardless of the interconnected nature of structural and electronic factors, the LHA−Rh^{I} PET switches can be treated as independent units amenable to synthetic modifications that tailor the structure−function relationship of the construct. As such, substitution of the central RC unit for other photoredox catalysts capable of being sensitized by Bodipy should retain the original allosteric regulatory properties of the construct. This suggests that WLA systems for chemical sensing and signal amplification[27] can be readily and generally designed to exhibit a desired catalytic response upon analyte detection. More broadly, our study shows that allosteric and in situ regulation of inorganic light-harvesting systems via structural and PET control is a highly malleable approach to the regulation of LHA−RC mimics.

EXPERIMENTAL SECTION

Materials and Methods. All synthetic procedures, characterization, and experiments were performed in a nitrogen atmosphere glovebox or in sealed containers under a stream of argon. All glassware, cuvettes, and cells were oven-dried for 24 h. Dichloromethane (CH_2Cl_2), acetonitrile, diethyl ether, and tetrahydrofuran (THF) solvents were transferred from an oxygen- and water-free solvent system (J. C. Meyer) into sealed containers and purged with a stream of argon for 20 min prior to use. 1,2-Dichlorobenzene and pentane were purchased as HPLC grade, similarly purged for 20 min with argon, and stored over activated molecular sieves. Deuterated solvents were purchased from Cambridge Isotope Laboratories and degassed with a stream of argon prior to use. The syntheses of the Bodipy ligand **6**,[20] model Bodipy−Rh^{I} complexes **M1** and **M2**,[19] **ImC$_{60}$**,[22] the porphyrin ligand **5**, complexes **(3**−**4)ImC$_{60}$**[7] and methyl viologen (MV) hexafluorophosphate[28] have been previously reported. 1-Benzyl-1,4-dihydronicotineamide (BNAH) was purchased from TCI Chemicals and used as received. All other chemicals were purchased from Aldrich Chemical Co. and used as received. ***Warning!*** *Tl^{+} and MV salts are extremely toxic and should be handled appropriately.* NMR spectra were recorded on a Bruker Avance 400 MHz. ^{1}H NMR spectra were referenced to residual proton resonances in deuterated solvents. ^{31}P{^{1}H} NMR spectra were referenced to an 85% H_3PO_4 aqueous solution. ^{19}F NMR spectra were referenced to a $CFCl_3$ sample in a $CDCl_3$ solution. ^{11}B{^{1}H} NMR spectra were referenced to neat BF_3·OEt_2. All chemical shifts are reported in ppm. High-resolution electrospray ionization (ESI) mass spectrometry (HRMS) spectra were recorded on an Agilent 6120 LC-TOF instrument in positive-ion mode.

UV−visible absorption measurements were performed with a Varian Cary 50 Bio spectrophotometer utilizing screw-cap 10-mm-cell-path quartz cuvettes (VWR). Steady-state fluorescence measurements were carried out in a Horiba Jovin-Yvonne Fluorolog fluorimeter, and fluorescence quantum yields were derived from a comparative method using sulforhodamine B in ethanol as the standard. In particular, quantum yields were calculated from the least-squares fit of integrated fluorescence emission versus absorbance value curves comprising seven dilution samples. Cyclic voltammetry measurements were performed with an Epsilon BASi potentiostat in an airtight cell comprising a glassy carbon working electrode, a silver wire pseudoreference electrode, and a platinum wire auxiliary electrode. Samples were prepared as 10 mM solutions in 0.1 M $N(nBu)_4PF_6$ in CH_2Cl_2. A scan rate of 100 mV/s was used in all measurements. All cyclic voltammetry graphs show potentials versus the ferrocene/ferrocenium (Fc/Fc^{+}) couple.

Titrations of **ImC$_{60}$** were studied via UV−visible spectroscopy at room temperature in a screw-cap cuvette with a total volume of 2 mL and a constant **1**−**2** concentration of 1 μM in CH_2Cl_2. Samples were prepared in a glovebox. Titrations were performed via the addition of aliquots of a 1 mM **ImC$_{60}$** solution in 1,2-dichlorobenzene into the solution of hosts **1**−**2**. Binding affinities (K_a) were calculated by monitoring the change in the absorbance at 434 nm, corresponding to the axially coordinated porphyrin's Soret band. Binding affinity values were obtained by nonlinear regression analysis of the binding curves utilizing the following equation:

$$\Delta\mathrm{Abs} = \varepsilon \times 0.5\left\{[\mathrm{G}] + [\mathrm{H}] + \frac{1}{K} - \sqrt{\left(x + [\mathrm{H}] + \frac{1}{K}\right)^2 - 4[\mathrm{H}][\mathrm{G}]}\right\}$$

Theoretical values for the energy-transfer efficiency were calculated from the overlap between the absorption spectrum of the porphyrin ligand **5** and the fluorescence spectra of either model complex **M1** or **M2** (Figures S17 and S18). Specifically, the emission spectra f_5 of either **M1** or **M2** and the molar absorption coefficient ε of **5** were used to calculate spectral overlap integral J using the following equation:

$$J = \int f_{\mathbf{M1-M2}}(\lambda)\, \varepsilon_{\mathbf{5}}(\lambda)\, \lambda^4\, \mathrm{d}\lambda$$

J values were then used to calculate the Forster distance values R_0, which were subsequently compared with the measured distances between the center of the Bodipy donor and the center of the porphyrin acceptor (R) in the crystal structure of **1** and the theoretical model of **2**. The rates of energy transfer were calculated by comparing in the excited-state lifetime values (τ) of the Bodipy antenna in model complexes **M1** and **M2** with complexes **1** and **2** using the following equation:

$$k_{\mathrm{EnT}} = (\tau_{\mathbf{1/2}})^{-1} - (\tau_{\mathbf{M1/M2}})^{-1}$$

Similarly, the rate of PET from Rh^{I} to the Bodipy excited state was calculated using the excited-state lifetime value of the Bodipy antenna in **M2** and **6** and the following equation:

$$k_{\mathrm{PET}} = (\tau_{\mathbf{M2}})^{-1} - (\tau_{\mathbf{6}})^{-1}$$

Photoredox Catalysis. Catalytic experiments were performed in screw-cap 10-mm-cell-path quartz cuvettes containing 0.1 mM methyl viologen hexafluorophosphate and 0.1 mM BNAH in CH_2Cl_2. MV was added from a concentrated methanolic solution. **ImC$_{60}$** was added from a concentrated 1,2-dichlorobenzene solution. In a typical experiment, the reagents, the Rh^{I} complex, **ImC$_{60}$**, and a stir bar were loaded into the cuvette in the dark inside a glovebox. The cuvette was placed inside a UV−visible spectrophotometer, and the solution was vigorously stirred with a magnetic stirrer. An encasing was built above the cuvette holder to provide a stream of argon while measurements were performed. A laser diode (PicoQuant) was placed inside the spectrophotometer perpendicular to the probe beam, and the excitation power was monitored regularly using a S130C slim photodiode power sensor connected to PM200 power and an energy meter console (Thorlabs). The redox reaction was monitored by

DOI: 10.1021/acs.inorgchem.6b00095
Inorg. Chem. XXXX, XXX, XXX−XXX

tracking absorbance changes at 630 nm, characteristic of reduced MV species. In order to add allosteric effectors to the reaction mixture, excitation was halted and the cuvette was taken into a glovebox and then returned to the spectrophotometer.

Experimental catalytic rate constants (k) were obtained from the least-squares fit of the kinetic curves produced by plotting the product concentration (derived from Beer's law) versus time. It was assumed that, at initial time intervals (i.e., t = 0−150 s), the reaction followed zero-order kinetics. Equation $[P] = kt + [P]_0$ was fit to the experimental value using the program *GraphPad* and employing an initial product concentration of 0 M.

Time-Resolved Optical Spectroscopy. Visible/NIR femtosecond TA spectroscopy was performed on an instrument that is described elsewhere.[29] Briefly, the 827 nm fundamental output of a commercial Ti:sapphire laser system (Tsunami oscillator/Spitfire amplifier, Spectra-Physics) was frequency-doubled to 414 nm (∼150 μJ/pulse). In our previous study, this beam was attenuated and used as the pump; here it is used to pump a seeded, two-stage, laboratory-constructed optical parametric amplifier (OPA). The signal output of the OPA was tuned to the desired wavelength, then attenuated, and chopped at 500 Hz. The single-filament continuum probe was generated by focusing into the appropriate nonlinear medium for the desired probe range. For a visible continuum (360−800 nm), a ∼1.5 μJ/pulse was tightly focused into a 5 mm cuvette containing a 1:1 mixture of H_2O/D_2O, while for the NIR probe (800−1600 nm), a ∼5 μJ/pulse was loosely focused into a proprietary source (Ultrafast Systems, LLC). The residual fundamental was filtered using an appropriate edge filter. Polarization of the pump beam was rotated to 54.7° ("magic" angle) relative to the horizontal probe. Both the pump and probe were focused to ∼100 μm at the sample. After interaction, the transmitted probe was then coupled into an optical fiber and detected using the appropriate detector (customized Helios, Ultrafast Systems, LLC).

TA signals were fit to a convolution of a Gaussian instrument response function with the sum of a multiexponential decay and a step function for signals extending far beyond the experimental window. Uncertainties are reported as the standard error of the fit.

Synthesis and Characterization. *[$Rh_2Cl_2(\kappa_2$-P,S-Bz-ZnP(mes)$_2$-Bz-κ_2-S,P)(P,S-F_4ph-Bodipy)$_2$] (**2**).* In a 25 mL vial equipped with a magnetic stir bar, Rh_2Cl_2(cyclooctene)$_4$ (3.6 mg, 0.005 mmol) was dissolved in a 1:1 solution of CH_2Cl_2/THF (3 mL). After stirring for 2 min, **5** (6.4 mg, 0.005 mmol) was added dropwise as a THF solution (3 mL). Immediately after, **6** (7.0 mg, 0.010 mmol) was added in a dropwise fashion as a CH_2Cl_2 solution (3 mL). The vial was then sealed and sonicated for 10 min to solubilize any precipitate. The solvent mixture was reduced to about 1 mL via evaporation in vacuo, and the product was precipitated via the addition of diethyl ether. The product was isolated via filtration through a Buchner funnel as a red solid (in situ $^{31}P\{^1H\}$ NMR; yield, 90%, isolated yield, 11 mg, 74%). ^1H NMR (400.16 MHz, 25 °C, CD_2Cl_2): δ 8.90−8.60 (m, 8 H), 8.36−7.95 (m, 8 H), 7.90−6.74 (m, 44 H), 4.71 (br s, 4 H), 3.30 (br s, 4 H), 2.89−0.90 (m, 74 H). $^{31}P\{^1H\}$ NMR (161.98 MHz, 25 °C, CD_2Cl_2): δ 65.1 (dd, $J_{P-P'}$ = 35 Hz, J_{P-Rh} = 71 Hz, 2 P), 64.0 ($J_{P-P'}$ = 35 Hz, J_{P-Rh} = 81 Hz, 2 P). ^{19}F NMR (376.49 MHz, 25 °C, CD_2Cl_2): δ −132.1 (q, J_{F-F} = 13 Hz, 4 F), −141.5 (q, J_{F-F} = 13 Hz, 4 F), −146.2 (q, J_{B-F} = 34 Hz, 4 F). $^{11}B\{^1H\}$ NMR (128.38 MHz, 25 °C, CD_2Cl_2): δ 0.06 (t, J_{B-F} = 33 Hz). HRMS(ESI$^+$). Calcd for $[M]^+$: m/z 2944.5964. Found: m/z 2944.5969.

*[$Rh_2(\kappa_2$-P,S-Bz-ZnP(mes)$_2$-Bz-κ_2-S,P)(κ_2-P,S-F_4ph-Bodipy)$_2$]OTf$_2$ (**1**).* In a 25 mL vial equipped with a magnetic stir bar, **2** (15 mg, 0.0050 mmol) was dissolved in CH_2Cl_2 (3 mL). Tl(OTf) (3.5 mg, 0.010 mmol) was added, and the suspension was stirred for 40 min. The sample was then filtered through a Buchner funnel, and the solvent was removed in vacuo, affording the product as a red solid (in situ $^{31}P\{^1H\}$ NMR; yields, quantitative; isolated yield, 14.9 mg, 94%). ^1H NMR (400.16 MHz, 25 °C, CD_2Cl_2): δ 8.88−8.63 (m, 8 H), 8.30 (d, J_{H-H} = 12 Hz, 4 H), 7.83 (d, J_{H-H} = 12 Hz, 4 H), 7.75−6.93 (m, 44 H), 4.47 (br s, 4 H), 3.27 (m, 4 H), 2.93−0.77 (m, 74 H). $^{31}P\{^1H\}$ NMR (161.98 MHz, 25 °C, CD_2Cl_2): δ 64.4 (dd, $J_{P-P'}$ = 36 Hz, J_{P-Rh} = 70 Hz, 2 P), 63.4 ($J_{P-P'}$ = 34 Hz, J_{P-Rh} = 78 Hz, 2 P). ^{19}F NMR (376.49 MHz, 25 °C, CD_2Cl_2): δ −78.9 (s, 6 F), −128.5 (q, J_{F-F} = 11 Hz, 4 F), −136.7 (q, J_{F-F} = 11 Hz, 4 F), −145.7 (q, J_{B-F} = 33 Hz, 4 F). $^{11}B\{^1H\}$ NMR (128.38 MHz, 25 °C, CD_2Cl_2): δ −0.02 (t, J_{B-F} = 32 Hz). HRMS(ESI$^+$). Calcd for $[M]^{+2}$: m/z 1437.3294. Found: m/z 1437.3287.

■ ASSOCIATED CONTENT

Supporting Information

The Supporting Information is available free of charge on the ACS Publications website at DOI: 10.1021/acs.inorgchem.6b00095.

Experimental details, including materials, methods, and synthetic protocols, optical spectra, titrations, control photoredox catalytic experiments, reversibility of allosterically induced structural changes, and NMR characterization. (PDF)

■ AUTHOR INFORMATION

Corresponding Authors

*E-mail: chadnano@northwestern.edu. Fax: (1) 847-467-5123.
*E-mail: m-wasielewski@northwestern.edu.

Present Address

§A.M.L.: Division of Chemistry and Chemical Engineering, California Institute of Technology, 1200 East California Boulevard, MC 127-72, Pasadena, California 91125, United States.

Author Contributions

The manuscript was written through contributions of all authors. All authors have given approval to the final version of the manuscript.

Notes

The authors declare no competing financial interest.

■ ACKNOWLEDGMENTS

This material is based on the work supported by the following awards: National Science Foundation Grant CHE-1149314 and U.S. Army Grant W911NF-11-1-0229. J.M.-A. acknowledges a fellowship from Consejo Nacional de Ciencia y Tecnologia. Time-resolved spectroscopy was supported as part of the ANSER Center, an Energy Frontier Research Center, funded by the U.S. Department of Energy, Office of Science, Office of Basic Energy Sciences, under Award DE-SC0001059 (to M.R.W. and R.M.Y.).

■ REFERENCES

(1) Wiester, M. J.; Ulmann, P. A.; Mirkin, C. A. *Angew. Chem., Int. Ed.* **2011**, *50*, 114−137.
(2) Goodey, N. M.; Benkovic, S. J. *Nat. Chem. Biol.* **2008**, *4*, 474−482.
(3) Kremer, C.; Lutzen, A. *Chem. - Eur. J.* **2013**, *19*, 6162−6196.
(4) Lifschitz, A. M.; Rosen, M. S.; McGuirk, C. M.; Mirkin, C. A. *J. Am. Chem. Soc.* **2015**, *137*, 7252−7261.
(5) Guillaume, S. M.; Kirillov, E.; Sarazin, Y.; Carpentier, J. F. *Chem. - Eur. J.* **2015**, *21*, 7988−8003.
(6) Kovbasyuk, L.; Kramer, R. *Chem. Rev.* **2004**, *104*, 3161−3187.
(7) Lifschitz, A. M.; Young, R. M.; Mendez-Arroyo, J.; Stern, C. L.; McGuirk, C. M.; Wasielewski, M. R.; Mirkin, C. A. *Nat. Commun.* **2015**, *6*, 6541.
(8) Raymo, F. M.; Tomasulo, M. *Chem. Soc. Rev.* **2005**, *34*, 327−336.
(9) Straight, S. D.; Kodis, G.; Terazono, Y.; Hambourger, M.; Moore, T. A.; Moore, A. L.; Gust, D. *Nat. Nanotechnol.* **2008**, *3*, 280−283.
(10) Kiss, A. Z.; Ruban, A. V.; Horton, P. *J. Biol. Chem.* **2008**, *283*, 3972−3978.

DOI: 10.1021/acs.inorgchem.6b00095
Inorg. Chem. XXXX, XXX, XXX−XXX

(11) Pascal, A. A.; Liu, Z. F.; Broess, K.; van Oort, B.; van Amerongen, H.; Wang, C.; Horton, P.; Robert, B.; Chang, W. R.; Ruban, A. *Nature* **2005**, *436*, 134−137.
(12) Ahn, T. K.; Avenson, T. J.; Ballottari, M.; Cheng, Y. C.; Niyogi, K. K.; Bassi, R.; Fleming, G. R. *Science* **2008**, *320*, 794−797.
(13) Scholes, G. D.; Fleming, G. R.; Olaya-Castro, A.; van Grondelle, R. *Nat. Chem.* **2011**, *3*, 763−774.
(14) Liddell, P. A.; Kodis, G.; Moore, A. L.; Moore, T. A.; Gust, D. *J. Am. Chem. Soc.* **2002**, *124*, 7668−7669.
(15) Terazono, Y.; Kodis, G.; Bhushan, K.; Zaks, J.; Madden, C.; Moore, A. L.; Moore, T. A.; Fleming, G. R.; Gust, D. *J. Am. Chem. Soc.* **2011**, *133*, 2916−2922.
(16) Pochorovski, I.; Breiten, B.; Schweizer, W. B.; Diederich, F. *Chem. - Eur. J.* **2010**, *16*, 12590−12602.
(17) Gilbert, M.; Esdaile, L. J.; Hutin, M.; Sawada, K.; Anderson, H. L.; Albinsson, B. *J. Phys. Chem. C* **2013**, *117*, 26482−26492.
(18) El-Khouly, M. E.; Fukuzumi, S.; D'Souza, F. *ChemPhysChem* **2014**, *15*, 30−47.
(19) Lifschitz, A. M.; Young, R. M.; Mendez-Arroyo, J.; Roznyatovskiy, V. V.; McGuirk, C. M.; Wasielewski, M. R.; Mirkin, C. A. *Chem. Commun.* **2014**, *50*, 6850−6852.
(20) Lifschitz, A. M.; Shade, C. M.; Spokoyny, A. M.; Mendez-Arroyo, J.; Stern, C. L.; Sarjeant, A. A.; Mirkin, C. A. *Inorg. Chem.* **2013**, *52*, 5484−5492.
(21) Yoo, H.; Rosen, M. S.; Brown, A. M.; Wiester, M. J.; Stern, C. L.; Mirkin, C. A. *Inorg. Chem.* **2012**, *51*, 11986−11995.
(22) D'Souza, F.; Smith, P. M.; Zandler, M. E.; McCarty, A. L.; Itou, M.; Araki, Y.; Ito, O. *J. Am. Chem. Soc.* **2004**, *126*, 7898−7907.
(23) Loudet, A.; Burgess, K. *Chem. Rev.* **2007**, *107*, 4891−4932.
(24) Guedes da Silva, M. F. C.; Trzeciak, A. M.; Ziolkowski, J. J.; Pombeiro, A. J. L. *J. Organomet. Chem.* **2001**, *620*, 174−181.
(25) Kobuke, Y. *Eur. J. Inorg. Chem.* **2006**, *2006*, 2333−2351.
(26) Fukuzumi, S.; Imahori, H.; Okamoto, K.; Yamada, H.; Fujitsuka, M.; Ito, O.; Guldi, D. M. *J. Phys. Chem. A* **2002**, *106*, 1903−1908.
(27) Masar, M. S.; Gianneschi, N. C.; Oliveri, C. G.; Stern, C. L.; Nguyen, S. T.; Mirkin, C. A. *J. Am. Chem. Soc.* **2007**, *129*, 10149−10158.
(28) Bockman, T. M.; Kochi, J. K. *J. Org. Chem.* **1990**, *55*, 4127−4135.
(29) Young, R. M.; Dyar, S. M.; Barnes, J. C.; Juricek, M.; Stoddart, J. F.; Co, D. T.; Wasielewski, M. R. *J. Phys. Chem. A* **2013**, *117*, 12438−12448.

DOI: 10.1021/acs.inorgchem.6b00095
Inorg. Chem. XXXX, XXX, XXX−XXX